Effective electron and hole masses in intrinsic and heavily n-type doped GaN and AlN

2001 J. Phys.: Condens. Matter 13 8915

(http://iopscience.iop.org/0953-8984/13/40/305)

INSTITUTE OF PHYSICS PUBLISHING JOURNAL OF PHYSICS: CONDENSED MATTER

J. Phys.: Condens. Matter **13** (2001) 8915–8922 PII: S0953-8984(01)24512-3

Effective electron and hole masses in intrinsic and heavily n-type doped GaN and AlN

C Persson[1], Bo E Sernelius[2], A Ferreira da Silva[3], R Ahuja[1] and B Johansson[1]

[1] Department of Physics, Box 530, University of Uppsala, SE-751 21 Uppsala, Sweden
[2] Solid State Division, Oak Ridge National Laboratory, Oak Ridge, Tennessee 37831-6032, USA
[3] Instituto de Fisica, Universidade Federal da Bahia, 40210-340 Salvador, Bahia, Brazil

Received 2 May 2001
Published 20 September 2001
Online at stacks.iop.org/JPhysCM/13/8915

Abstract

We have investigated the electronic structure near the band edges in intrinsic and heavily n-type doped GaN and AlN. Both the wurtzite and the zinc-blende polytypes have been considered. The electronic structures of the intrinsic materials were obtained from a full-potential linearized augmented plane wave calculation. We show the importance of performing a fully relativistic calculation. For instance, the hole mass in cubic AlN is a very large and negative quantity if spin–orbit coupling is excluded, whereas the fully relativistic calculation gives a relatively small and positive value. The electron–phonon coupling was taken into account according to the Fröhlich Hamiltonian for large polarons, resulting in effective polaron masses. The effects on the effective electron masses due to doping were investigated by using a Green's function formalism within the random phase approximation and with a local-field correction according to Hubbard.

1. Introduction

GaN and AlN are wide-band-gap semiconductor materials with low compressibility, good thermal stability and with chemical and radiation inertness [1]. Because of the recent progress in crystal growth, high-quality thin films of cubic structures can now be produced, which opens up further technological applications involving the group III nitrides. However, there is still a lack of knowledge on the basic electronic properties of both the wurtzite (wz) and the zinc-blende (zb) polytypes of GaN and AlN.

Band structure calculations of intrinsic group III nitrides have been reported, mainly on wz-GaN and wz-AlN. For instance, Kim *et al* [3] have presented a full-potential linearized muffin-tin orbital calculation by employing the atomic sphere approximation. Although their band structures agree fairly well with the present results for the conduction-band minimum (CBM), they found that zb-AlN has a valence-band maximum (VBM) along the [110]-direction,

and thus not at the Γ-point. In the present work we have performed first-principle full-potential band structure calculations of wz-GaN, wz-AlN, zb-GaN and zb-AlN. We present the crystal-field splitting, the spin–orbit splitting, and the effective electron and hole masses. The hole masses in particular are affected by the spin–orbit interaction. For instance, we also find that zb-AlN has a large, negative hole-mass component at the Γ-point for the uppermost valence band if the spin–orbit interaction is excluded (hence, the VBM is not at the Γ-point), but with the spin–orbit coupling the hole mass becomes positive and the VBM is now at the Γ-point.

The Hamiltonian of the intrinsic materials $\hat{H}_0$ describes the interactions between the ions and the electrons of the crystal, and solving the eigenvalue problem results in the single-electron energies $E_j^0(\boldsymbol{k})$. In an n-type semiconductor, the crystal also consists of donors which can be ionized, either thermally or by metal–non-metal phase transition. The ionized donors give rise to a 'gas' of free electrons in the conduction band. Now, the crystal electrons interact strongly with the electron gas and with the ionized donors. Since the nitrides are polar materials, these interactions are screened by the optical phonons. The additional interactions can be treated as a perturbation to $\hat{H}_0$. The eigenvalue problem of the total Hamiltonian results in the modified electron energies $E_j(\boldsymbol{k})$, where $\Delta E_j(\boldsymbol{k}) = \mathrm{Re}\,[E_j(\boldsymbol{k}) - E_j^0(\boldsymbol{k})]$ is the self-energy. In this paper we investigate how much these doping-induced interactions modify the effective electron masses.

2. Computational method

The calculation of the electronic structure of the intrinsic materials is based on a relativistic, full-potential linearized augmented plane wave (FPLAPW) method [4], choosing the exchange-correlation potential of Perdew *et al* [5], derived within the generalized gradient approximation (GGA). More information of the computational method can be found in [6].

The FPLAPW method does not include lattice dynamics. In polar materials the electrons interact relatively strongly with the longitudinal optical phonons. We have therefore included the electron–optical phonon coupling according to the Fröhlich Hamiltonian [7]. The polaron energy for large polarons is given by

$$E_j^{pol}(\boldsymbol{k}) = -\mathrm{Re}\int \frac{\mathrm{d}\boldsymbol{q}}{(2\pi)^3}\int \frac{\mathrm{d}\omega}{2\pi\,\mathrm{i}}\sum_{j'}\Lambda_{j,j'}(\boldsymbol{k},\boldsymbol{k}')\left\{\left[\frac{\upsilon(\boldsymbol{q})}{\varepsilon_\infty}-\frac{\upsilon(\boldsymbol{q})}{\kappa(\omega)}\right]\right.$$
$$\left.\times\frac{1}{2}\left(\frac{1}{\omega+\omega_{j,j'}(\boldsymbol{k},\boldsymbol{k}')-\mathrm{i}\delta}-\frac{1}{\omega-\omega_{j,j'}(\boldsymbol{k},\boldsymbol{k}')+\mathrm{i}\delta}\right)\right\} \tag{1}$$

where $\boldsymbol{k}' = \boldsymbol{k}+\boldsymbol{q}$, $\omega_{j,j'}(\boldsymbol{k},\boldsymbol{k}') = (E_{j'}^0(\boldsymbol{k}') - E_j^0(\boldsymbol{k}))/\hbar$, and $\Lambda_{j,j'}(\boldsymbol{k},\boldsymbol{k}')$ is the overlap integral for the periodic part of the Bloch functions [8, 9].

The investigation of the doping-induced effects on the energy dispersions has been performed by using a zero-temperature Green's function formalism [7]. A full description of the perturbation Hamiltonian can be found in [7, 10], so here we will only give the resulting expressions for the self-energy, which is described in terms of the unperturbed Green's function $G_j^0(\boldsymbol{k},\omega)$and the dielectric function $\tilde{\varepsilon}(\boldsymbol{q},\omega)$ of the electron gas. Within the random phase approximation with the Hubbard's local-field correction $\bar{f}(\boldsymbol{q})$, the dielectric function of the electron gas is given by [7–10]

$$\tilde{\varepsilon}(\boldsymbol{q},\omega) = 1-\left(1-\frac{\bar{f}(\boldsymbol{q})}{\nu}\right)\frac{2}{\hbar}\int\frac{\mathrm{d}\boldsymbol{k}}{(2\pi)^3}\int\frac{\mathrm{d}\omega'}{2\pi\,\mathrm{i}}\frac{\upsilon(\boldsymbol{q})}{\kappa(\omega)}G_{c1}^0(\boldsymbol{k},\omega')G_{c1}^0(\boldsymbol{k}+\boldsymbol{q},\omega'+\omega) \tag{2}$$

where $\upsilon(\boldsymbol{q})/\kappa(\omega)$ is the Coulomb potential screened by the optical phonons and the intrinsic crystal [7–10]. The CBM is very parabolic in all materials considered here [6], and we have

therefore used parabolic energy dispersion in equation (2), which means that the integral can be solved analytically [8]. The self-energy is given by [8, 10]

$$\Delta E_j(\boldsymbol{k}) = -\mathrm{Re}\int \frac{\mathrm{d}\boldsymbol{q}}{(2\pi)^3}\int \frac{\mathrm{d}\omega}{2\pi\,\mathrm{i}}\sum_{j'}\Lambda_{j,j'}(\boldsymbol{k},\boldsymbol{k}')\frac{\upsilon(\boldsymbol{q})}{\kappa(\omega)}\left\{\frac{G^0_{j'}(\boldsymbol{k}',\omega+E^0_j(\boldsymbol{k})/\hbar)}{\tilde{\varepsilon}(\boldsymbol{q},\omega)}\right.$$
$$\left.+\frac{1}{2}\left(\frac{1}{\omega+\omega_{j,j'}(\boldsymbol{k},\boldsymbol{k}')-\mathrm{i}\delta}-\frac{1}{\omega-\omega_{j,j'}(\boldsymbol{k},\boldsymbol{k}')+\mathrm{i}\delta}\right)\right\}$$
$$+\mathrm{Re}\int \frac{\mathrm{d}\boldsymbol{q}}{(2\pi)^3}\left(\frac{N_D}{\hbar}\right)\left(\frac{\upsilon(\boldsymbol{q})}{\kappa_0\tilde{\varepsilon}(\boldsymbol{q},0)}\right)^2\sum_{j'}\Lambda_{j,j'}(\boldsymbol{k},\boldsymbol{k}')G^0_{j'}(\boldsymbol{k}',E^0_j(\boldsymbol{k})/\hbar). \qquad (3)$$

The first term in (3) is the exchange-correlation contribution, the second term is a subtraction of the electrostatic self-interactions, and the last term comes from the electron–impurity ion interaction.

3. Lattice parameters and band gaps

The lattice parameters a c, and u were obtained by minimizing the total energy (see [6]). The fundamental band gap of intrinsic semiconductors E^0_g is normally underestimated in the LDA and GGA. Here, the direct band gap of wz-GaN (wz-AlN) is calculated to be $E^0_g = 1.92$ (4.20) eV, whereas the corresponding measured value is 3.50 (6.28) eV (see [6] for a complete reference list of the experimental data). Also, the band gap of zb-GaN is direct: $E^0_g = 1.83$ eV and the experimental value is about 3.2 eV (see [6] for a complete reference list of the experimental data). In zb-AlN the calculated CBM is at the X-point with $E^0_g = 3.32$ eV. We have estimated a band-gap correction Δ_g according to the quasi-particle model of Bechstedt and Del Sole [11]. The corrected band gaps are close to the experimental values: $E^0_g + \Delta_g = 3.55$, 6.05, 3.44, and 5.17 eV in wz-GaN, wz-AlN, zb-GaN, and zb-AlN, respectively.

4. Effective electronic masses

The effective electronic masses were calculated for the lowest conduction band ($c1$) and for the three uppermost valence bands ($v1$, $v2$, and $v3$). The effective masses of the intrinsic material were determined directly from the energy dispersions of the FPLAPW calculation. The corresponding effective polaron masses are given by the second derivative of $(E^0_j(\boldsymbol{k})+E^{pol}_j(\boldsymbol{k}))$, with respect to $\boldsymbol{k}$ and the doping-dependent effective masses are given by the second derivative of $(E^0_j(\boldsymbol{k}) + E^{pol}_j(\boldsymbol{k}) + \Delta E_j(\boldsymbol{k}))$, [8].

4.1. Electron masses in wz-GaN and wz-AlN

In both wz-GaN and wz-AlN, the electron mass tensor can be represented by a transverse $m_{c1,\perp}$ and a longitudinal $m_{c1,\parallel}$ mass. The calculated effective electron masses are presented in table 1. Our calculated values for wz-GaN are $m_{c1,\perp} = 0.18m_0$ and $m_{c1,\parallel} = 0.16m_0$, and the corresponding calculated polaron masses are $m^{pol}_{c1,\perp} = 0.19m_0$ and $m^{pol}_{c1,\parallel} = 0.17m_0$, which are close to the experimental results of $m_{c1,\perp} = m_{c1,\parallel} = 0.22m_0$ and $0.222m_0$ (see [6] for a complete reference list of the experimental data). Earlier calculations [2, 3] of the bare electron masses in wz-GaN and wz-AlN give similar results to those presented here.

In table 1 we also present the electron masses for the dopant concentrations $N_D = 1\times10^{18}$ and 1×10^{19} cm^{-3}. The mass values at the CBM are much smaller than in the intrinsic materials.

Table 1. Effective intrinsic (intr), polaron (pol), and doping-induced ($N_D = 1 \times 10^{18}$ and 1×10^{19} cm^{-3}) electron masses in wz-GaN and wz-AlN at the CBM and at the Fermi energy ($\boldsymbol{k}_F$).

	wz-GaN				wz-AlN			
Electrons	intr	pol	1×10^{18}	1×10^{19}	intr	pol	1×10^{18}	1×10^{19}
$m_{c1,\perp}$ (m_0)	0.18	0.19	0.09	0.06	0.30	0.33	0.21	0.14
$m_{c1,\parallel}$ (m_0)	0.16	0.17	0.08	0.05	0.29	0.32	0.21	0.13
$m^{kF}_{c1,\perp}$ (m_0)			0.16	0.17			0.25	0.28
$m^{kF}_{c1,\parallel}$ (m_0)			0.14	0.15			0.24	0.27

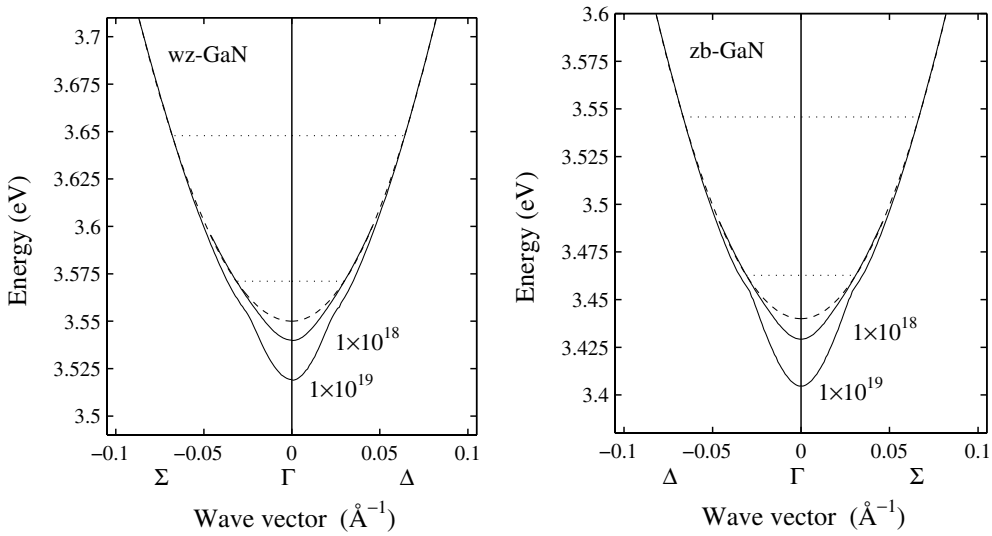

Figure 1. The electronic band structure near the CBM for intrinsic (broken curve) and heavily doped (full curves) wz-GaN and zb-GaN.

However, near the Fermi wavevector ($\boldsymbol{k}_F$) the masses are almost unchanged. The doping-induced effects on the effective masses can be explained by looking at the energy dispersion for wz-GaN (figure 1(a)). The broken curve represents the lowest conduction band for intrinsic wz-GaN. The full curves are the band curvatures for $N_D = 1 \times 10^{18}$ and 1×10^{19} cm^{-3} and the horizontal broken lines represent the corresponding Fermi levels. The full curves have been shifted by -23 (-49) meV for $N_D = 1 \times 10^{18}$ (1×10^{19}) cm^{-3} in order to make the comparison. One clearly sees band tailoring effects coming from the $\boldsymbol{k}$-dependent self-energy (we have not considered any localized impurity states). The very non-parabolic curvature for $N_D = 1 \times 10^{19}$ cm^{-3} at $\hbar\omega_{LO}$ below the Fermi energy is characteristic for heavily doped polar semiconductors [10]. In figure 2(a) we show how the masses at the CBM and at the Fermi energy depend on the donor concentrations. The tailoring effect becomes stronger as the concentration is increased. At a concentration of about 9×10^{18} cm^{-3}, the Fermi energy becomes equal to $\hbar\omega_{LO}$, which directly affects the electron masses at the CBM.

Table 2. Same as in table 1, but for zb-GaN and zb-AlN.

	zb-GaN				zb-AlN			
Electrons	intr	pol	1×10^{18}	1×10^{19}	intr	pol	1×10^{18}	1×10^{19}
$m_{c1,\perp}$ (m_0)	0.16	0.17	0.07	0.06	0.32	0.36	0.58	0.13
$m_{c1,\parallel}$ (m_0)					0.52	0.59	0.94	0.21
$m^{kF}_{c1,\perp}$ (m_0)			0.14	0.16			0.46	0.29
$m^{kF}_{c1,\parallel}$ (m_0)							0.74	0.47

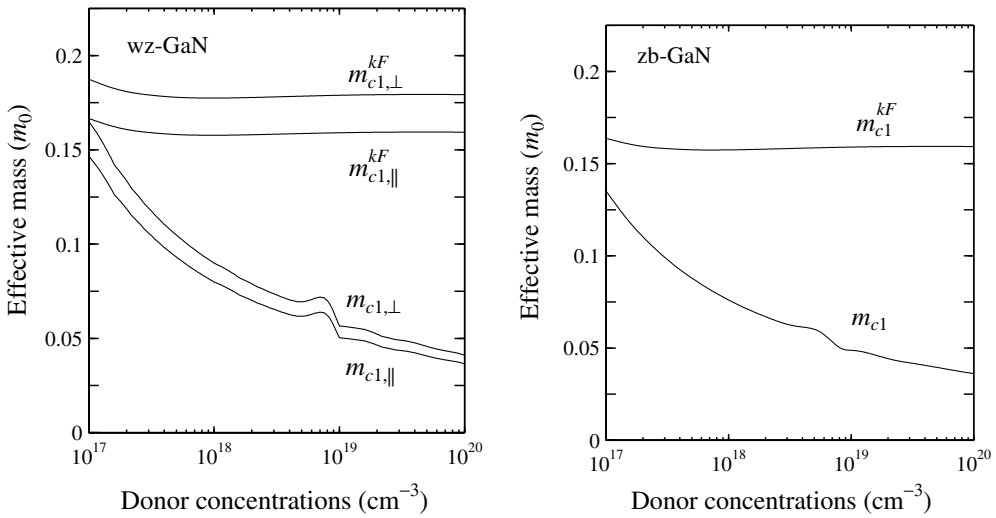

Figure 2. Doping-dependent electron masses in (a) wz-GaN and (b) zb-GaN at the CBM and at the Fermi energy ($\boldsymbol{k}_F$).

4.2. Electron masses in zb-GaN and zb-AlN

The electron mass tensor in zb-GaN is represented by a single mass component m_{c1}, and in zb-AlN by transverse $m_{c1,\perp}$ and longitudinal $m_{c1,\parallel}$ masses (table 2). To the best of our knowledge, there are no experimental values for theses polytypes. In figures 1(b) and 2(b) we present the corresponding result for zb-GaN as for wz-GaN in the previous section.

4.3. Hole masses in wz-GaN and wz-AlN

A detailed band structure of the three (six if spin is considered) uppermost valence bands in wz-GaN and wz-AlN is presented in figures 3(a) and 3(b) by the full curves. The spin–orbit interaction causes the splitting with $\Delta_{so} = 4.8$ meV in wz-GaN and $\Delta_{so} = 13$ meV in wz-AlN. In GaN the two uppermost bands have Γ_7 and Γ_9 symmetry and the third crystal-field split-off band has Γ_7 symmetry and is about 32 meV below the second band. In AlN it is different. The uppermost band is the crystal-field split-off band with Γ_7 symmetry and the two bands with Γ_7 and Γ_9 symmetry are about 210 meV below the uppermost band.

The broken curves in figure 3 represent the energy dispersions when the spin–orbit interaction is excluded. Even though the spin–orbit interaction splits up the bands by only 5–8 meV, the interaction has a strong affect on the effective hole masses. For instance, the transverse hole mass of the uppermost (second uppermost) valence band in zb-GaN (zb-AlN)

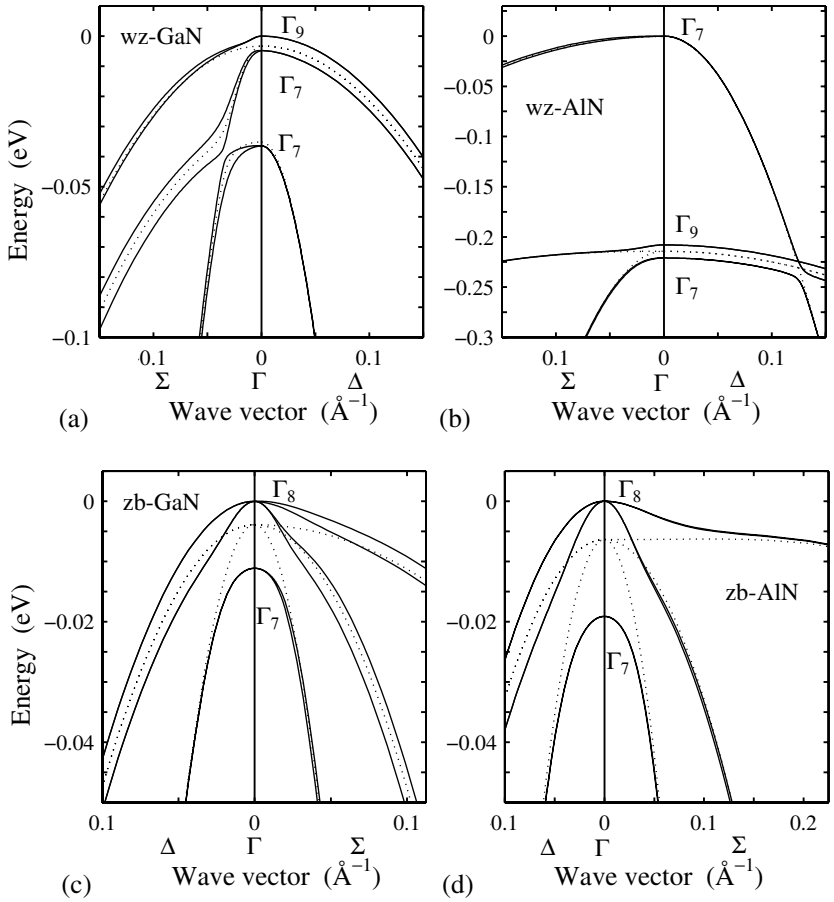

Figure 3. The electronic band structure near the VBM in (a) wz-GaN, (b) wz-AlN, (c) zb-GaN, and (d) zb-AlN. The broken curves represent the energy dispersions in the absence of spin–orbit interaction.

is $2.22m_0$ ($17.20m_0$) if the spin–orbit interaction is excluded, and $0.32m_0$ ($4.46m_0$) if the spin–orbit interaction is included. However, the longitudinal mass of this band is less affected by the spin–orbit interaction.

There is a lack of experimental data for the valence bands in GaN and AlN. The measured hole mass $m_{v1} = 0.60$–$0.80m_0$ (see [6] for a complete reference list of the experimental data) in wz-GaN agrees roughly with our density-of-states mass $(m_{v1,\parallel}m_{v1,\perp}m_{v1,\perp})^{1/3} = 0.68m_0$, where the polaron interaction is included.

4.4. Hole masses in zb-GaN and zb-AlN

The band structures of the three uppermost valence bands in zb-GaN and zb-AlN are shown in figures 3(c) and 3(d). The spin–orbit splitting is $\Delta_{so} = 11$ meV in zb-GaN and $\Delta_{so} = 19$ meV in zb-AlN. This splitting affects the valence bands strongly in the vicinity of the Γ-point. The broken curves represent the energy dispersions when the spin–orbit interaction is excluded. Noticeable is the strong effect on the two uppermost valence bands in the ΓK-direction for zb-AlN. Without spin–orbit coupling the VBM is about 10% away from the Γ-point in this

Table 3. Same as in table 1, but for hole masses at the VBM.

	wz-GaN		wz-AlN		
Holes	intr	pol	intr	pol	
$m_{v1,\perp}$ (m_0)	0.32	0.36		4.46	5.83
$m_{v1,\parallel}$ (m_0)	2.10	2.40		0.25	0.33
$m_{v2,\perp}$ (m_0)	0.32	0.36		0.61	0.75
$m_{v2,\parallel}$ (m_0)	1.28	1.44		3.56	4.39
$m_{v3,\perp}$ (m_0)	1.08	1.23		0.59	0.72
$m_{v3,\parallel}$ (m_0)	0.15	0.17		3.47	4.26

Table 4. Same as in table 3, but for zb-GaN and zb-AlN.

	zb-GaN		zb-AlN	
Holes	intr	pol	intr	pol
$m_{v1}(\Gamma X)$ (m_0)	0.90	1.10	1.44	2.02
$m_{v1}(\Gamma K)$ (m_0)	1.58	1.93	3.06	4.29
$m_{v1}(\Gamma L)$ (m_0)	1.98	2.42	4.38	6.14
$m_{v2}(\Gamma X)$ (m_0)	0.22	0.24	0.44	0.49
$m_{v2}(\Gamma K)$ (m_0)	0.21	0.23	0.38	0.43
$m_{v2}(\Gamma L)$ (m_0)	0.21	0.23	0.37	0.42
$m_{v3}(\Gamma X)$ (m_0)	0.35	0.39	0.67	0.78
$m_{v3}(\Gamma K)$ (m_0)	0.35	0.39	0.66	0.77
$m_{v3}(\Gamma L)$ (m_0)	0.35	0.39	0.66	0.77
m_{v1} (m_0)	1.30		2.53	
m_{v2} (m_0)	0.21		0.38	
m_{v3} (m_0)	0.36		0.67	

direction. Furthermore, the band is very flat. This results in a large and negative hole-mass component for the uppermost valence band at the Γ-point: $m_{v1}(\Gamma K) = -253.07 m_0$ (and $m_{v2}(\Gamma K) = 1.44 m_0$). However, by including the spin–orbit interaction, and thereby forcing the bands to split, the VBM is at the Γ-point with a positive mass value: $m_{v1}(\Gamma K) = 3.06 m_0$ (and $m_{v2}(\Gamma K) = 0.38 m_0$). Thus, it is crucial to include the spin–orbit coupling for determining the effective hole masses (table 4). The spherical average values (m_{v1}, m_{v2}, and m_{v3}) have been determined according to [12].

5. Conclusions

We have calculated the band structure of wz- and zb-GaN and -AlN using a relativistic, FPLAPW method. The energy dispersions and the effective electronic masses near the fundamental band gap are presented. The calculated valence-band splittings, effective electron and hole masses are in good agreement with available experimental results.

We have seen strong effects on the VBM due to the spin–orbit interaction, especially in the zb structures. A correct treatment of the band splitting of the degeneracy is thus necessary for investigating the hole masses, even for light materials. By doping the materials heavily, one can distort the CBM strongly. At a donor concentration of $N_D = 1 \times 10^{19}$ cm^{-3} the effective electron masses at the CBM and at the Fermi level differ by about 50–70%.

Acknowledgments

This work was financially supported by the Swedish Research Council for Engineering Sciences (TFR), the US Department of Energy under contract No DE-AC05-00OR22725 with Oak Ridge National Laboratory, managed by UT-Battelle, LLC, and the Brazilian National Research Council (CNPq).

References

[1] Strite S and Morkoç H 1992 *J. Vac. Sci. Technol.* B **10** 1237
[2] Suzuki M, Uenoyama T and Yanase A 1995 *Phys. Rev.* B **52** 8132
[3] Kim K, Lambrecht W R L, Segall B and van Schilfgaarde M 1997 *Phys. Rev.* B **56** 7363
[4] Blaha P, Schwarz K and Luitz J 1999 *WIEN97, A Full Potential Linearized Augmented Plane Wave Package for Calculating Crystal Properties* (Wien, Austria: Karlheinz Schwarz, Technisch Universität Wien) ISBN 3-9501031-0-4
[5] Perdew J P, Burke K and Ernzerhof M 1996 *Phys. Rev. Lett.* **77** 3865
[6] Persson C, Ferreira da Silva A, Ahuja R and Johansson B 2001 *J. Cryst. Growth* accepted
[7] Mahan G D 1990 *Many-Particle Physics* 2nd edn (New York: Plenum)
[8] Persson C, Lindefelt U and Sernelius B E 1999 *Phys. Rev.* B **60** 16 479
[9] Persson C, Lindefelt U and Sernelius B E 1999 *J. Appl. Phys.* **86** 4419
[10] Sernelius B E 1987 *Phys. Rev.* B **36** 4878
[11] Bechstedt F and Del Sole R 1988 *Phys. Rev.* B **38** 7710
[12] Persson C and Lindefelt U 1997 *J. Appl. Phys.* **82** 5496